AGU PUBLICATIONS

Global Biogeochemical Cycles

RESEARCH ARTICLE
10.1002/2013GB004652

Key Points:
- Trichodesmium populations simulated with an eddy resolving model
- Simulating observed biomass and nitrogen fixation requires enhanced export
- Model captures observed association of Trichodesmium with anticyclonic eddies

Supporting Information:
- Readme
- Supporting Information Figures S1–S4, Table S1

Correspondence to:
D. J. McGillicuddy Jr.,
dmcgillicuddy@whoi.edu

Citation:
McGillicuddy, D. J., Jr. (2014), Do *Trichodesmium* spp. populations in the North Atlantic export most of the nitrogen they fix?, *Global Biogeochem. Cycles, 28*, doi:10.1002/2013GB004652.

Received 15 MAY 2013
Accepted 16 JAN 2014
Accepted article online 22 JAN 2014

Do *Trichodesmium* spp. populations in the North Atlantic export most of the nitrogen they fix?

Dennis J. McGillicuddy Jr.[1]

[1]Department of Applied Ocean Physics and Engineering, Woods Hole Oceanographic Institution, Woods Hole, Massachusetts, USA

Abstract A new observational synthesis of diazotrophic biomass and nitrogen fixation provides the opportunity for systematic quantitative evaluation of these aspects in biogeochemical models. One such model of the Atlantic Ocean is scrutinized, and the simulated biomass is found to be an order of magnitude too low. Initial attempts to increase biomass levels through decreasing grazing and other loss terms caused an unrealistic buildup of nitrate in the upper ocean. Two key changes to the model structure facilitated a closer match to the observed biomass and nitrogen fixation rates: addition of a pathway for export of diazotrophically fixed organic material and uptake of inorganic nitrogen by the diazotroph population. These changes, along with a few other revisions to existing model parameterizations, facilitate more accurate simulation of basin-scale distributions of diazotrophic biomass, as well as mesoscale variations contained therein. The resulting solutions suggest that the *Trichodesmium* spp. populations of the North Atlantic export the vast majority of the nitrogen they fix, a finding that awaits assessment through direct observation.

1. Introduction

Nitrogen fixation by cyanobacteria of the genus *Trichodesmium* constitutes an important input into the global nitrogen cycle [*Carpenter*, 1983; *Capone et al*., 1997; *Karl et al*., 2002]. As such, modeling the abundance, distribution, and productivity of these populations offers an important tool for quantification of the associated fluxes of nitrogen and their impacts on ecosystems and climate. A number of prior studies have documented realistic simulations of diazotrophic biomass and nitrogen fixation on basin to global scales [*Coles et al*., 2004; *Hood et al*., 2004; *Coles and Hood*, 2007; *Moore and Doney*, 2007; *Monteiro et al*., 2010, 2011; *Dutkiewicz et al*., 2012]. However, a recent global compilation and synthesis of observations [*Luo et al*., 2012] provide the opportunity for more thorough evaluation of models of this type. Herein direct comparisons are made between one such model of the Atlantic Ocean and the new observational synthesis. Although prior simulations [*Anderson et al*., 2011] were able to capture the large-scale patterns described by *Luo et al*. [2012], diazotrophic biomass was underestimated by an order of magnitude in the high-abundance region of the tropics and southern Sargasso Sea. Revisions to the model are described that allow for closer agreement between simulated and observed distributions of diazotrophs, both in terms of basin-scale biogeography as well as mesoscale variations. A key change in the model structure is a direct pathway for vertical export of *Trichodesmium* spp., which allows the solution to reach the observed levels of biomass and nitrogen fixation while avoiding unrealistic buildup of nitrate in the surface ocean.

2. Model Description

The physical model is the Los Alamos Parallel Ocean Program (POP) [*Smith et al*., 2000] version 2.0.1. The spatial grid is an eddy-resolving (0.1° longitude × 0.1° cos(latitude)) North Atlantic domain (20°S to 72°N, 98°W to 17°E) with 42 *z* coordinate levels. Configuration of the physical simulation is identical to that of *Anderson et al*. [2011], as is the coarse resolution implementation (1.6° longitude × 1.6° cos(latitude); 40 levels in the vertical) used for parameter dependence and sensitivity analysis.

The biological/chemical component is based on a 24 state variable version of the "Biogeochemical Elemental Cycling" (BEC) model [*Moore et al*., 2002, 2004, 2006; *Moore and Doney*, 2007; *Doney et al*., 2009] as modified by *Anderson et al*. [2011]. The model has three phytoplankton groups (Figure S1 of the supporting information): diatoms, small phytoplankton, and N_2-fixing diazotrophs (DIAZ). Although diazotrophic organisms in the ocean are comprised by a diverse assemblage of taxa [*LaRoche and Breitbarth*, 2005; *Zehr*, 2011], the

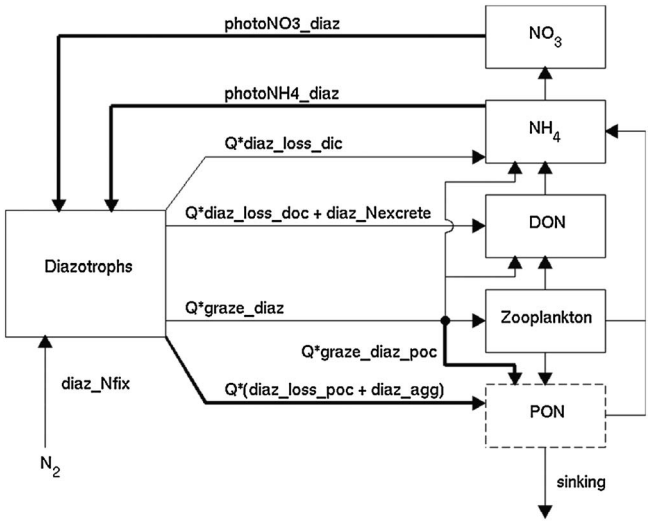

Figure 1. Schematic of the simulated diazotrophic nitrogen cycle. Fluxes added to the present model are indicated in bold, whereas thin lines indicate fluxes present in both prior and current versions. The dashed box for PON reflects the fact that it is not a true state variable, insofar as that the material is assumed to sink and remineralize instantly.

colonial cyanobacteria *Trichodesmium* spp. tends to dominate in terms of biomass and nitrogen fixation in the Atlantic region of primary interest in this study [*Goebel et al*., 2010]. Thus, for the present purposes, the terms diazotroph and *Trichodesmium* spp. are used interchangeably. Model phytoplankton, zooplankton, and sinking particulate organic matter (POM) have constant C/N/P ratios, but variable content of Fe and Chl (for all phytoplankton), $CaCO_3$ (for small phytoplankton), and SiO_2 (for diatoms). The limiting nutrients are NO_3, NH_4, PO_4, Fe, and for diatoms SiO_3. The remaining biological state variables are O_2, dissolved inorganic carbon (DIC), alkalinity, dissolved organic carbon, dissolved organic nitrogen, dissolved organic phosphorus, and dissolved organic iron. The biological model is coupled to and run concurrently with the physical model. The multidimensional positive definite centered difference advection scheme is used for biological tracers [*Oschlies and Garcon*, 1999], and its implementation in the POP model is described by *McGillicuddy et al*. [2003].

In an attempt to better match the observations, the one-dimensional Regional Testbed model [*Friedrichs et al*., 2007] was set up at contrasting locations: the Bermuda Atlantic Time-Series Study (BATS) site where *Trichodesmium* spp. abundance is relatively low and in the tropics where it is much higher. The Regional Testbed software includes an optimization algorithm that permits fitting parameters simultaneously among the selected sites. The optimized parameters were then tested in coarse resolution (1.6°) three-dimensional simulations. Because optimal parameters derived in a one-dimensional setting are not necessarily optimal in a three-dimensional environment, additional sensitivity experiments were carried out in the coarse resolution model to improve upon the parameter choices derived from the Regional Testbed. This was an iterative process that included not only refinements within the existing model structure, but also revisions to the model structure itself (Figure 1 and Table S1 of the supporting information). Both aspects are described in turn below.

Several parameterizations within the prior model structure were modified. First, the factor specifying temperature dependence on diazotroph growth rate was changed from a Q_{10}-type relationship $T_{\mathrm{func\_diaz}} = 2^{(T-30)/10}$ to a functional fit of laboratory experiments (using an isolate of *Trichodesmium erythraeum*) described by *Breitbarth et al*. [2007]. The data suggest a quasi-parabolic dependence of growth rate on temperature within the interval between 18°C and 36°C, with maximal growth at 26.9°C. To represent this, a temperature anomaly T_a is defined relative to the optimal temperature $T_a = \max(18, \min(36, T)) - 26.9$ to model the temperature dependence with $T_{\mathrm{func\_diaz}} = \max(0, 1 - 0.0215 * T_a^2 + 0.000109 * T_a^4)$ such that $T_{\mathrm{func\_diaz}}$ is zero outside the temperature window and rises to a value of one at the optimal temperature. Qualitatively, this provides a good fit to the data presented in Figure 1 in the work of *Breitbarth et al*. [2007].

Second, the parameterization of iron scavenging by adsorption onto particles was updated from that described by *Moore and Doney* [2007] to *Moore and Braucher* [2008]. The primary difference between them is that the

definition of the sinking mass onto which scavenging occurs is expanded from particulate organic carbon (POC) and mineral dust to include biogenic silica and calcium carbonate components. In addition, the scaling factor for scavenging at high iron concentrations was increased in order to bring the near-surface iron concentrations into better agreement with observations. Half-saturation constants for iron uptake by small phytoplankton and diatoms were updated to values used in version 1.0.4 of the Community Earth System Model (CESM; http://www.cesm.ucar.edu). The half-saturation constant by iron uptake by diazotrophs was increased to 0.8 nM. Although this value is a bit high relative to experimental assays [*Berman-Frank et al*., 2001], it helps compensate for the continued overestimation of near-surface iron concentrations despite the improved scavenging parameterization mentioned above.

Third, the mortality and grazing losses of diazotrophs were modified in an attempt to rectify the systematic overestimation of *Trichodesmium* spp. biomass in the subtropics and underestimation in the tropics. In the *Anderson et al*. [2011] solution, diazotroph concentrations over most of the subtropical gyre were near their mortality threshold concentration, below which mortality and grazing losses do not occur. The threshold value used in that simulation was higher than observed concentrations of *Trichodesmium* spp. in the subtropics (see *Orcutt et al*. [2001], and references therein) and was therefore lowered to the same value used for small phytoplankton and diatoms. To ameliorate the underestimation of biomass in the tropics, grazing and mortality rates, which are among the least constrained parameters, were lowered. Justification for the former lies in that relatively few copepod species appears to graze *Trichodesmium* spp., most notably the harpacticoid copepod *Macrosetella gracilis* [*O'Neil and Roman*, 1994]. As for the latter, the mortality rate for *Trichodesmium* spp. probably should not be higher than that used for small phytoplankton and diatoms (0.1 d^{-1}).

Although these changes to the model parameters resulted in an intermediate solution with improved representations of *Trichodesmium* spp. biomass and nitrogen fixation, there was an unintended consequence: unrealistic accumulation of nitrate in near-surface waters of the high-biomass regions. Increased abundance and productivity of the *Trichodesmium* spp. population led to increased supply of biologically fixed nitrogen, through remineralization of both particulate and dissolved organic material. This in turn caused a regional shift from nitrogen to phosphorus limitation in the phytoplankton community, resulting in buildup of nitrate in surface waters to unrealistic levels (>1 μM) in those areas. In order to simulate the high biomass and nitrogen fixation rates in the tropics and southern subtropical gyre without building up excess nitrate in surface waters, two structural changes to the model were made.

First, a separate parameterization for export of diazotrophically derived particulate organic matter was added. An observational basis for this revision consists of isotopic data suggesting penetration of biologically fixed light nitrogen into the main thermocline via sinking particles at station ALOHA in the Pacific [*Karl et al*., 1997; *Dore et al*., 2002; *Casciotti et al*., 2008]—although the source of that material may be primarily nitrogen-fixing endosymbionts living within diatoms rather than *Trichodesmium* spp. [*Karl et al*., 2012]. In the model, the sources of diazotrophic POM include both grazing losses and mortality; a quadratic term was added to the latter to create an aggregation term like those for small phytoplankton and diatoms. All of the diazotroph mortality and 27.5% of diazotroph grazing losses go to POM. As in prior implementations of the BEC model, the N/P ratio of diazotrophs is assumed to be 50:1 to reflect the supra-Redfield ratio observed in natural populations of *Trichodesmium* spp. [*Letelier and Karl*, 1998]. However, there is evidence for plasticity in this ratio from both laboratory experiments and field samples [*Krauk et al*., 2006; *White et al*., 2006]. The C/N ratio in diazotrophs is close to Redfield, the same as that used for the sinking flux of small phytoplankton, diatoms, and zooplankton. In contrast to the treatment of other POM in the model, diazotrophic POM does not include ballasting by SiO_2, $CaCO_3$, or lithogenic minerals. Thus, the sinking flux of diazotrophic carbon $POCt_{flux}$ has only a single unprotected, unballasted component:

$$POCt_{flux}(z+dz) = POCt_{flux}(z)\exp(-dz/(POCt\_diss/T_{funcP})) + POCt_{prod} * (1 - \exp(-dz/(POCt\_diss/T_{funcP}))) POCt\_diss/T_{funcP}$$

where the remineralization length scale POC*t*_diss is distinct from that used for other "soft" fractions of the export flux. Numerical experiments in the one-dimensional test bed framework suggested a value of 300 m for POC*t*_diss provided the best fit to observations, although the solutions were not particularly sensitive to that precise value.

A second change to the model structure allowed for uptake of inorganic nitrogen by diazotrophs, a pathway that has also been implemented in the CESM 1.0 version of the BEC [*Moore et al*., 2013]. It has been known for some time that *Trichodesmium* spp. is capable of taking up both nitrate and ammonium [*Goering et al*., 1966], yet the partitioning of uptake among the various forms of nitrogen, including dissolved organic forms, is still not fully understood [*Mulholland et al*., 2001]. Based on continuous culture experiments by *Holl and Montoya* [2005] that document preferential uptake of nitrate over dinitrogen, diazotrophs in the model first take up what they can in the form of nitrate and ammonium and then meet any remaining need by fixing nitrogen. Unfortunately, the extant literature does not provide direct estimates of the half-saturation constants for uptake, although nitrate uptake has been observed in experimental amendments as low as 0.03–1.0 μM [*Mulholland et al*., 2001]. Following *Moore et al*. [2013], values for the half-saturation constants for nitrate and ammonium uptake are chosen to be significantly larger (2X and 10X, respectively) than those for small phytoplankton, so that diazotrophs do not compete with that group for dissolved inorganic nitrogen in the oligotrophic open ocean.

3. Experimental Design

The coupled physical-biological simulation was initialized with climatological temperature, salinity, and nutrients, and with previous model results for the rapidly adjusting biological variables, as described by *Anderson et al*. [2011]. The simulation was run for 14.5 years with a 6 h, repeating "normal year" atmospheric forcing [*Large and Yeager*, 2004], during which time it reached quasi equilibrium. The biological model changes mentioned above were then made, the nutrients (NO_3, PO_4, SiO_3, and O_2) reinitialized with World Ocean Atlas July distributions [*Garcia et al*., 2006a, 2006b] and the coupled model run for 7 more years. Only the last 4 years of simulation are analyzed, after the biological fields (excluding DIC, alkalinity, and O_2, which in this model do not affect the other biological variables) reached a new quasi equilibrium. Model output was saved in 5 day averages.

4. Basin-Scale Patterns in Biomass and Nitrogen Fixation

The simulation of *Trichodesmium* spp. biomass (Figure 2, top) captures many of the large-scale features present in the *Luo et al*. [2012] synthesis. The solution is improved over the prior results described by *Anderson et al*. [2011] (Figure S2 of the supporting information). In particular, near-surface biomass in the high-abundance region of the tropics and southern subtropical gyre is closer to observed concentrations. The model also predicts high concentrations in the Gulf Stream and its eastward extension into the North Atlantic. Although this feature is not resolved by the in situ database, it is evident in satellite observations [*Westberry and Siegel*, 2006].

Despite the overall improvement in the fidelity of the simulated biomass, some discrepancies remain—such as overestimation east of South America at 10–15°S and in the 28–32°N latitude band of the Sargasso Sea. Another area of apparent bias in the model is located off west Africa in the latitude band 10–20°N, where the simulation seems to systematically exceed the observations. Repeated transects in April/May and September/October reveal consistently high biomass in this area from the equator to 15°N [*Tyrrell et al*., 2003], although the binned annual averages computed by *Luo et al*. [2012] show considerable spatial variability in that vicinity.

The large-scale patterns in nitrogen fixation (Figure 2, bottom) generally mimic those of biomass. Differences between the revised and prior solutions are less dramatic than in the biomass fields (Figure S3 of the supporting information), but there are improvements. For example, the northern boundary of the high-fixation region in the tropics (yellow-to-green transition in Figure 2 (bottom)) is shifted northward, bringing the simulated rates into better agreement with the observations in the southern limb of the subtropical gyre. Enhanced nitrogen fixation is also evident in the Gulf Stream region, bringing the simulation into closer agreement with observations off the coast of northeastern North America. There are some areas in which model predictions of nitrogen fixation are degraded, such as in the northeast Atlantic where previously well-simulated rates are underestimated (Figure S3 of the supporting information).

Although the high biomass and rates of nitrogen fixation in the western tropical Atlantic are relatively well captured in the model, the river plume dynamics thought to be important to nitrogen fixation in that area [*Borstad*, 1982; *Lenes et al*., 2005] are not. Specifically, *Subramaniam et al*. [2008] describe how the Amazon

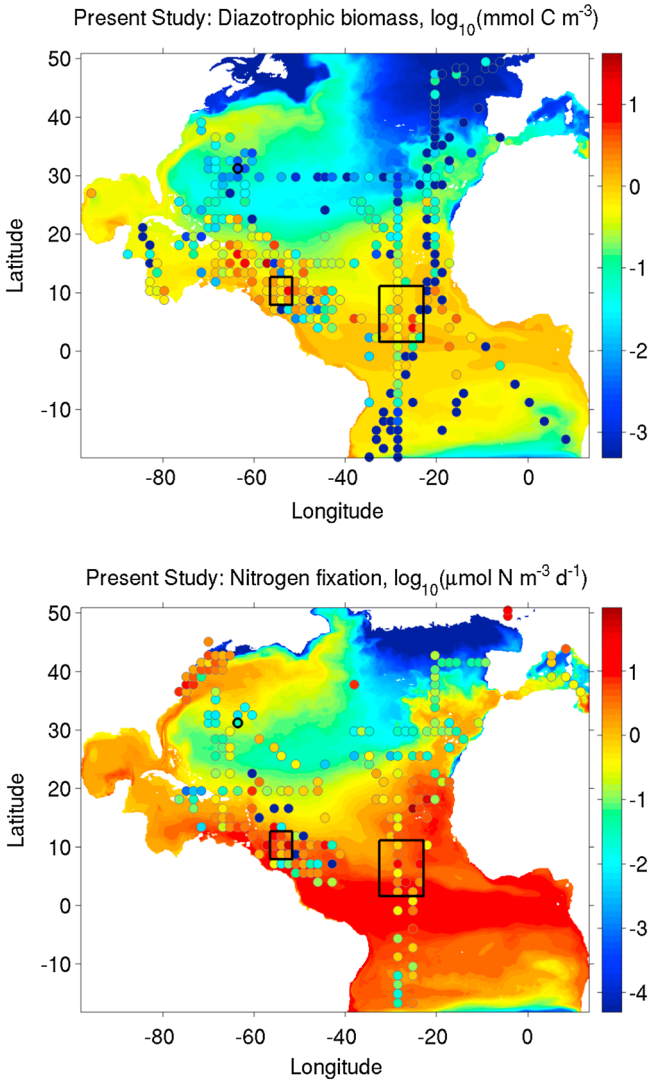

Figure 2. Simulated near-surface (0–10 m) (top) diazotrophic biomass and (bottom) nitrogen fixation. Data from *Luo et al.* [2012], binned onto the 1.6° model grid, are shown as colored circles. Outlined in black are the locations of BATS (circle near 32°N, 64°W), as well as tropical west (rectangle centered at 10°N, 54°W) and tropical east (rectangle centered at 6°N, 28°W) domains, for which detailed flux diagnosis is presented in Figure 4.

River outflow stimulates nitrogen fixation both by diatom-diazotroph assemblages as well as *Trichodesmium* spp. in different stoichiometric niches within the plume, which can extend more than 1000 km from the river mouth. Neither of these two nitrogen-fixing regimes is represented in this model, insofar as riverine influences are parameterized by restoring surface salinity to climatological values. As such, freshwater fluxes are prescribed, but the associated nutrient and micronutrient inputs are not.

Another important caveat with respect to assessment of the simulated rates arises from a recently discovered bias in an established isotopic method for measure nitrogen fixation [*Großkopf et al.*, 2012]. Typically, $^{15}N_2$ tracer is introduced as a gas bubble which is assumed to rapidly equilibrate with the liquid phase. Direct comparisons with a new approach using dissolved $^{15}N_2$ gas challenge that assumption, indicating that the gas bubble method significantly underestimates nitrogen fixation. Because this method is used in much of the data that comprise the *Luo et al.* [2012] analysis for the Atlantic, the observational estimates with which the model results are compared (Figure 2, bottom) may have to be revised upward by as much as a factor of two.

5. Controls on the Simulated Diazotrophic Populations

Over most of the high-abundance region of the tropical and subtropical North Atlantic, diazotrophic populations are regulated by the availability of phosphorus (Figure 3), a pattern roughly consistent with predecessors of this model [*Moore et al.*, 2004; cf. their Figure 7]. North of that area, temperature exerts the primary control, although there is a narrow zonal band of iron limitation associated with the Gulf Stream and its extension (see section 7 below). From the equator south, iron generally limits diazotrophy in the model with the exception of a small region in the vicinity of 10°S, 20°W. Qualitatively similar large-scale patterns in phosphorus and iron limitation of diazotrophs are predicted by a biogeographical model driven by nutrient supply stoichiometry [*Ward et al.*, 2013; cf. their Figure 7].

Phosphorus limitation of diazotrophic populations in the high-abundance region of the North Atlantic is consistent with the notion of ample iron supply from aeolian deposition of dust particles originating from African deserts [*Fung et al.*, 2000; *Berman-Frank et al.*, 2001; *Mahowald et al.*, 2005; *Moore et al.*, 2009]. Moreover, a wide variety of assays on natural populations from this region indicate phosphorus stress, including cell quota measurements [*Sañudo-Wilhelmy et al.*, 2001] and quantification of alkaline phosphatase activity [*Dyhrman et al.*, 2002; *Webb et al.*, 2007; *Mather et al.*, 2008; *Sohm et al.*, 2008; *Hynes et al.*, 2009].

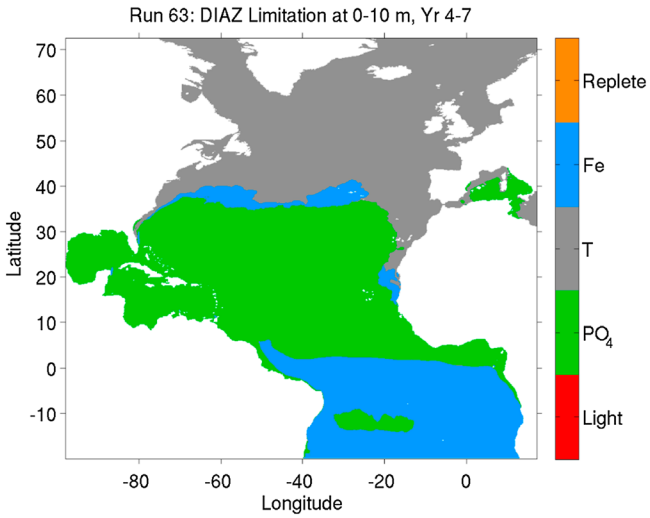

Figure 3. Most limiting factor for growth of the simulated diazotrophic population in near-surface (0–10 m) waters, averaged over the final 4 years of the simulation: iron (Fe), temperature (*T*), phosphate (PO_4), and light.

Selective remineralization of phosphorus from the dissolved organic material pool is also indicative of phosphorus limitation [*Clark et al*., 1998], and *Trichodesmium* colonies appear to have complex consortia of epibionts that serve precisely this purpose [*Van Mooy et al*., 2012]. Experimental incubations with additions of inorganic phosphorus can stimulate nitrogen fixation [*Webb et al*., 2007], although results from the eastern tropical North Atlantic suggest colimitation by phosphorus and iron [*Mills et al*., 2004]. Abundances of iron-binding photosynthetic and nitrogen-fixing proteins in natural populations of *Trichodesmium* spp. in the North Atlantic are also consistent with iron stress [*Richier et al*., 2012].

6. Nitrogen Fluxes

Detailed nitrogen budgets for three of the most densely sampled sites (Figure 4) further illustrate the improvement in simulated diazotrophic biomass. Whereas biomass was underestimated by an order of magnitude in the tropical west and tropical east domains of the *Anderson et al*. [2011] solution, biomass in the present simulation is much closer, albeit still smaller, than observed. Diazotrophic biomass also increased at BATS, degrading the solution at that location. However, biomass at BATS is still an order of magnitude smaller than in tropical areas and thus still qualitatively consistent with observed large-scale biogeography of *Trichodesmium* spp. Nitrogen fixation also increased, eclipsing the observed means in all three sites. However, given the high variability in the observations, the simulated rates at the tropical sites are not unrealistic. Nitrogen fixation is no doubt overestimated at BATS, but is an order of magnitude less than in the high-abundance region. As mentioned above, upward revision of nitrogen fixation rate estimates based on $^{15}N_2$ assimilation measurements [*Großkopf et al*., 2012] could bring the simulation and observations into closer agreement.

Nitrogen fluxes are significantly reorganized in the present model (Figure 4). The most significant change is the large amount of diazotrophic biomass that is converted into particulate organic nitrogen (PON) and subsequently exported, a pathway not available in the prior model. At the tropical sites, 70–75% of the nitrogen fixed by diazotrophs is exported by this process. This was a key addition to the model formulation, allowing for higher standing stocks of diazotrophic biomass while avoiding unrealistic buildup of inorganic nitrogen via remineralization within the euphotic zone. Unrealistic buildup of inorganic nitrogen was also ameliorated by allowing for uptake of nitrate and ammonium by diazotrophs, a pathway that supplies 15–20% of the diazotrophic nitrogen utilization at the tropical sites.

7. Mesoscale Variations

To assess eddy-driven fluctuations in the simulated populations of *Trichodesmium* spp., mesoscale features were identified by local extrema in sea level anomaly (SLA) computed from the 5 day averages of model output. Model-based SLA was defined by the residual after removing the large-scale spatial trends by a symmetric two-dimensional Gaussian filter with a 3° longitude *e*-folding scale and a 7.5° maximum radius. Following *Anderson et al*. [2011], each eddy was classified as one of four types according to the sign of their SLA and the sense of the isopycnal displacement at the base of the euphotic zone (taken to be 97 m): regular cyclones ("C"; negative SLA and positive density anomaly at 97 m), regular anticyclone ("A"; positive SLA and negative density anomaly), mode-water eddy ("M"; positive SLA and positive density anomaly), and "thinny" ("T"; negative SLA and negative density anomaly). The term thinny derives from the fact that in the Sargasso

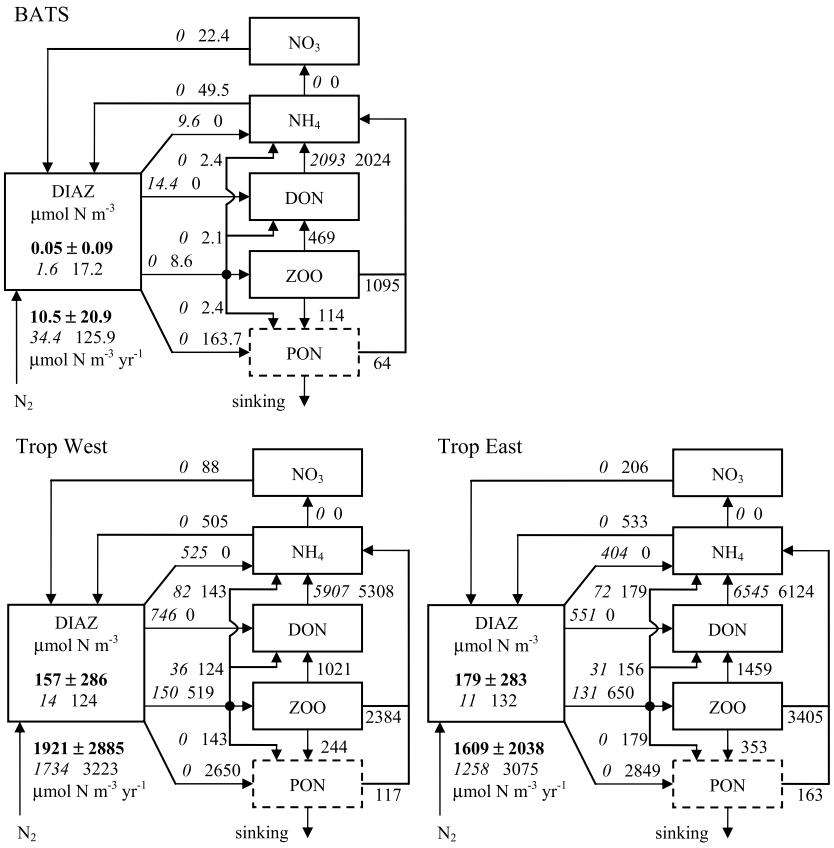

Figure 4. Annual mean surface (0–10 m) diazotroph-related nitrogen budget at the locations shown in Figure 2. Fluxes between boxes are in μmol N m^{-3} yr^{-1}. Diazotroph biomass values are shown inside the DIAZ box. Observed values and standard deviations are in bold, the work of *Anderson et al.* [2011] in italics, and the new model results shown in regular font.

Sea, these eddies have a relatively thin layer of 18° mode water between the seasonal and main thermoclines, whereas in "mode-water" eddies that layer is anomalously thick. In both cases, displacement of the main thermocline dominates the SLA and associated surface geostrophic velocity, such that thinnies are cyclonic and mode-water eddies are anticyclonic.

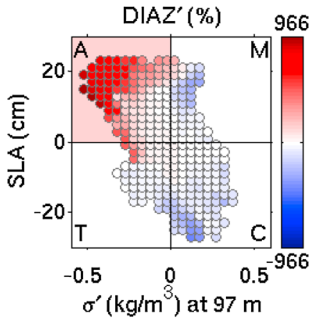

Figure 5. Vertically integrated (0–104 m) diazotrophic biomass anomalies (mg C m^{-2}), expressed as percent anomaly from the large-scale mean, binned according to SLA and in situ density anomaly at 97 m in the subdomain bordered by the white rectangle in Figure 6 (30–35°N, 30–48°W). The four quadrants correspond to anticyclones (A), mode-water eddies (M), thinnies (T), and cyclones (C). The background shading indicates the observed correlations in this region, which suggest the enhancement of *Trichodesmium* spp. populations in anticyclones [*Davis and McGillicuddy*, 2006]. For consistency with the observations, analysis of the model output is restricted to the August–September time frame.

The model simulates realistic mesoscale variations in *Trichodesmium* spp. populations. For example, *Davis and McGillicuddy* [2006] noted enhancements of *Trichodesmium* spp. populations in anticyclones within the subtropical gyre, with local abundance anomalies of up to an order of magnitude. This aspect was not captured in the *Anderson et al.* [2011] solution (Figure S4 of the supporting information), yet is clearly evident in the present simulation (Figure 5). Because the observations were collected in the August–September time frame, the analysis of the model solutions is restricted to that time interval. Of the 4 years that were analyzed, the association of positive biomass anomalies with anticyclones was most pronounced in year two (not shown). A synoptic (5 day) snapshot during that time period illustrates the nature of the association:

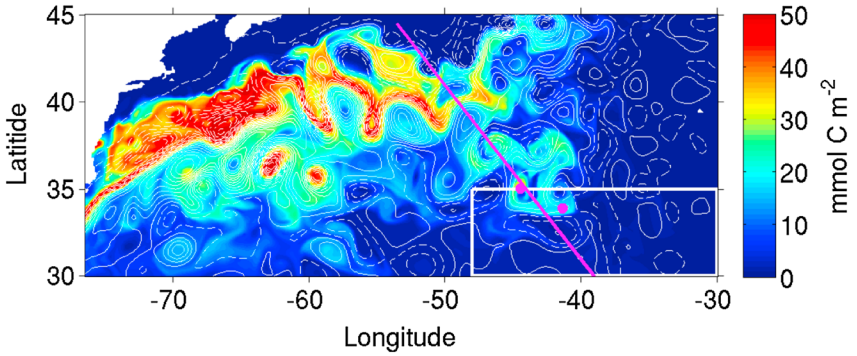

Figure 6. Vertically integrated (0–104 m) diazotrophic biomass (color) with isolines of sea level anomaly overlayed (contour interval of 6 cm; solid corresponds to +3 cm and above, dashed to −3 cm and below). Fields are averaged over the 5 day period, 8–12 September in year 18 of the simulation. White rectangle indicates the area of comparison with observations from *Davis and McGillicuddy* [2006]. Magenta dots indicate two anticyclonic features with enhanced diazotrophic biomass (see text). Location of the transect shown in Figure 8 is depicted as a magenta line. Note that sea level anomaly has been smoothed with a Gaussian-weighted running average with an *e*-folding scale of four grid points and a maximum cutoff of 10 points (1° longitude).

anticyclonic eddy features derived from the Gulf Stream extension region carry high biomass into the north-northwestern region of the observational domain (Figure 6). Biomass in the Gulf Stream and its extension was much lower in the *Anderson et al*. [2011] solution (Figure S2 of the supporting information), which may explain why the association with anticyclones was not present in that simulation.

Based on the snapshot presented in Figure 6, it is clear that the eddy-driven transport of *Trichodesmium* spp. biomass plays a role in generating the association with anticyclones. However, that does not discount the possibility of local eddy-induced enhancement of the population. To investigate this, a composite anticyclone was created by averaging all such features within the space/time domain of interest in eddy-centric coordinates. Indeed, there is a local enhancement of growth rate within these anticyclones (Figure 7a). Analysis of the limitation terms in the diazotrophic growth rate equation reveals that they are limited by phosphate in the upper ocean and temperature below (Figure 7b). The shallower temperature limitation horizon in the interior of the eddies suggests relief from phosphorus limitation, and phosphate in the lower euphotic zone (60–100 m) is on average higher in the interiors of anticyclones in this region (Figure 7c). In fact, the phosphorus enhancement is sufficient to shift the population toward iron limitation in an isolated area at 60 m depth at approximately 50 km radius (Figure 7b).

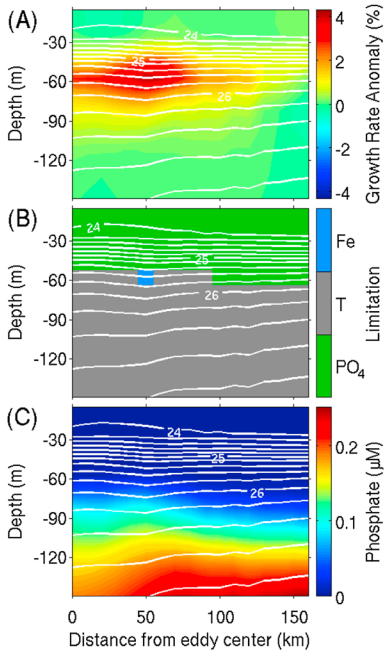

Figure 7. (a) Diazotrophic-specific growth rate anomaly, (b) limitation factors, and (c) phosphate concentrations in anticyclones with high diazotrophic biomass located within the white rectangle in Figure 6 (30–35°N, 30–48°W) during August–September. Two such features are identified by magenta dots in the snapshot shown in Figure 6. Radial averages were constructed from synoptic snapshots of model output using local maxima in sea level anomaly to define the positions of eddy centers. In each panel, density (σ_θ) contours are overlayed in white.

What is the source of the excess phosphate in these anticyclones? A transect from the high-abundance region in the Gulf Stream through the domain of interest (magenta line in Figure 6) reveals a gradient in phosphate with concentrations increasing to the northwest, particularly at depth (Figure 8, bottom). This large-scale gradient is consistent with the climatology used to initialize the model nutrient fields. Detailed comparison of the vertical section with

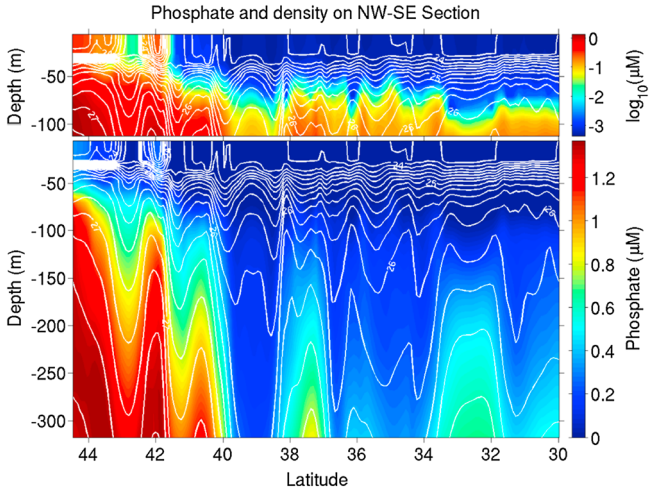

Figure 8. Phosphate section (color) along the magenta line in Figure 6, averaged over the 5 day period, 8–12 September of year 18 in the simulation, the year during which diazotrophic biomass anomalies were most pronounced in anticyclones. Density (σ_0) contours are overlayed in white at intervals of 0.2 kg m^{-3}. (top) The 0–110 m concentrations are plotted on a log scale; (bottom) the 0–320 m concentrations are plotted on a linear scale.

the phenomenology in SLA and diazotrophic biomass in Figure 6 suggests eddy-driven transport of phosphate which in turn drives local enhancement at the base of the euphotic zone (Figure 8, top). This finding is consistent with the suggestion by *Palter et al.* [2011] that excess phosphate supplied from the Gulf Stream system is a key source of nutrition for nitrogen fixation in the subtropics. Their study stressed the importance of wind-driven Ekman transport and isopycnal mixing in phosphate transport, estimating the eddy-induced fluxes to be small and upgradient via a parameterization derived from the work of *Gent et al.* [1995]. This eddy-resolving simulation suggests that the downgradient transport by the eddies provides an additional mechanism of phosphate supply which would add to those described by *Palter et al.* [2011]. In the simulation, the supply of phosphate from the Gulf Stream system is sufficient to transform the northern periphery of the subtropical gyre from phosphorus limitation to iron limitation of diazotrophic populations (Figure 3).

8. Conclusions

In this model, large export fluxes of diazotrophically derived material are required to sustain observed nitrogen fixation rates while maintaining realistic nutrient gradients in the upper ocean. Unfortunately, there do not appear to be any direct measurements in the high-biomass region of the North Atlantic that can be used to test this hypothesis—although the relative paucity of *Trichodesmium* spp. found in sediment traps has led some to conclude that their sinking flux is small [*Mulholland*, 2007]. However, recent laboratory experiments simulating bloom termination with *T. erythraeum* IMS101 suggest that the primary fate of the bloom material and its associated products was sinking to the bottom of the experimental chamber [*Bar-Zeev et al.*, 2013]. While observations of the vertical flux of *Trichodesmium* spp. are scarce, there is ample isotopic evidence that diazotrophically derived material makes its way into the food web [*Montoya et al.*, 2002], suspended particulate matter [*Landrum et al.*, 2011], sinking particles [*Capone et al.*, 1998], and deepwater nitrate [*Knapp et al.*, 2008]. Furthermore, supra-Redfield ratios of nitrate to phosphate in the main thermocline of the North Atlantic imply substantial rates of nitrogen fixation and subsequent export of that material [*Lipschultz and Owens*, 1996; *Michaels et al.*, 1996; *Gruber and Sarmiento*, 1997; *Hansell et al.*, 2004]. Reconciliation of these various imprints of nitrogen fixation on near-surface and deep ocean properties will require a mechanistic understanding of the nature of export flux of diazotrophically derived material, for which an expanded observational basis is essential.

Similarly, the effects of mesoscale ocean dynamics on diazotrophy are just beginning to come into focus. This simulation suggests that the eddy-induced transport of *Trichodesmium* spp. populations and the excess phosphorus from the Gulf Stream region can potentially explain the observed association with anticyclones in the northern subtropical gyre [*Davis and McGillicuddy*, 2006]. However, this is also just a hypothesis that awaits evaluation with direct observations of the nutrient environment in such features, as no such

measurements were available in the prior study. Enhancement of *Trichodesmium* spp. in anticyclones has also been noted in other regions, such as the eastern North Atlantic [*González Taboada et al.*, 2010] and oligotrophic North Pacific [*Fong et al.*, 2008; *Church et al.*, 2009]. In both cases, the mechanism of enhancement is different than that described herein, and future studies of mesoscale variations in such populations are likely to reveal a wide variety of physical-biological interactions.

Acknowledgments
Support of this research by the National Science Foundation and the National Aeronautics and Space Administration is gratefully acknowledged. I thank Laurence Anderson for carrying out the simulations and for providing technical assistance in their analysis. T.S. Bibby, S.C. Doney, J.K. Moore, Y. Luo, and B. Van Mooy all provided helpful feedback. I greatly appreciate the constructive critiques by three referees and Associate Editor, which helped improve an earlier version of the manuscript.

References

Anderson, L. A., D. J. McGillicuddy, M. E. Maltrud, I. D. Lima, and S. C. Doney (2011), Impact of eddy–wind interaction on eddy demographics and phytoplankton community structure in a model of the North Atlantic Ocean, *Dyn. Atmos. Oceans*, *52*(1-2), 80–94, doi:10.1016/j.dynatmoce.2011.01.003.

Bar-Zeev, E., I. Avishay, K. D. Bidle, and I. Berman-Frank (2013), Programmed cell death in the marine cyanobacterium *Trichodesmium* mediates carbon and nitrogen export, *ISME J.*, *7*, 1–9, doi:10.1038/ismej.2013.121.

Berman-Frank, I., J. T. Cullen, Y. Shaked, R. M. Sherrell, and P. G. Falkowski (2001), Iron availability, cellular iron quotas, and nitrogen fixation in *Trichodesmium*, *Limnol. Oceanogr.*, *46*(6), 1249–1260.

Borstad, G. A. (1982), The influence of the meandering Guiana Current on surface conditions near Barbados- temporal variations of *Trichodesmium* (Cyanophyta) and other plankton, *J. Mar. Res.*, *40*, 435–452.

Breitbarth, E., A. Oschlies, and J. LaRoche (2007), Physiological constraints on the global distribution of *Trichodesmium* – effect of temperature on diazotrophy, *Biogeosciences*, *4*, 53–61, doi:10.5194/bg-4-53-2007.

Capone, D. G., J. P. Zehr, H. W. Pearl, B. Bergman, and E. J. Carpenter (1997), *Trichodesmium*, a globally significant marine cyanobacterium, *Science*, *276*, 1221–1229.

Capone, D. G., A. Subramaniam, J. P. Montoya, M. Voss, C. Humborg, A. M. Johansen, R. L. Siefert, and E. J. Carpenter (1998), An extensive bloom of the N_2-fixing cyanobacterium *Trichodesmium erythraeum* in the central Arabian Sea, *Mar. Ecol. Prog. Ser.*, *172*, 281–292.

Carpenter, E. J. (1983), Nitrogen fixation by marine *Oscillatoria* (*Trichodesmium*) in the world's oceans, in *Nitrogen in the Marine Environment*, edited by E. J. Carpenter and D. G. Capone, pp. 65–103, Academic Press, New York.

Casciotti, K. L., T. W. Trull, D. M. Glover, and D. Davies (2008), Constraints on nitrogen cycling at the subtropical North Pacific Station ALOHA from isotopic measurements of nitrate and particulate nitrogen, *Deep Sea Res., Part II*, *55*(14–15), 1661–1672, doi:10.1016/j.dsr2.2008.04.017.

Church, M. J., C. Mahaffey, R. M. Letelier, R. Lukas, J. P. Zehr, and D. M. Karl (2009), Physical forcing of nitrogen fixation and diazotroph community structure in the North Pacific subtropical gyre, *Global Biogeochem. Cycles*, *23*, GB2020, doi:10.1029/2008GB003418.

Clark, L. L., E. D. Ingall, and R. Benner (1998), Marine phosphorus is selectively remineralized, *Nature*, *393*(6684), 426–426.

Coles, V. J., and R. R. Hood (2007), Modeling the impact of iron and phosphorus limitations on nitrogen fixation in the Atlantic Ocean, *Biogeosciences*, *4*, 455–479.

Coles, V. J., R. R. Hood, M. Pascual, and D. G. Capone (2004), Modeling the impact of *Trichodesmium* and nitrogen fixation in the Atlantic Ocean, *J. Geophys. Res.*, *109*, C06007, doi:10.1029/2002JC001754.

Davis, C. S., and D. J. McGillicuddy (2006), Transatlantic abundance of the N_2-fixing colonial cyanobacterium *Trichodesmium*, *Science*, *312*, 1517–1520.

Doney, S. C., I. Lima, J. K. Moore, K. Lindsay, M. J. Behrenfeld, T. K. Westberry, N. Mahowald, D. M. Glover, and T. Takahashi (2009), Skill metrics for confronting global upper ocean ecosystem-biogeochemistry models against field and remote sensing data, *J. Mar. Syst.*, *76*(1-2), 95–112.

Dore, J. E., J. R. Brum, L. M. Tupas, and D. M. Karl (2002), Seasonal and interannual variability in sources of nitrogen supporting export in the oligotrophic subtropical North Pacific Ocean, *Limnol.Oceanogr.*, *47*(6), 1595–1607.

Dutkiewicz, S., B. A. Ward, F. Monteiro, and M. J. Follows (2012), Interconnection of nitrogen fixers and iron in the Pacific Ocean: Theory and numerical simulations, *Global Biogeochem. Cycles*, *26*, GB1012, doi:10.1029/2011GB004039.

Dyhrman, S. T., E. A. Webb, D. M. Anderson, J. Moffett, and J. Waterbury (2002), Cell specific detection of phosphorus stress in *Trichodesmium* from the Western North Atlantic, *Limnol. Oceanogr.*, *47*, 1832–1836.

Fong, A. A., D. M. Karl, R. Lukas, R. M. Letelier, J. P. Zehr, and M. J. Church (2008), Nitrogen fixation in an anticyclonic eddy in the oligotrophic North Pacific Ocean, *ISME J.*, *2*(6), 663–676.

Friedrichs, M. A. M., et al. (2007), Assessment of skill and portability in regional marine biogeochemical models: Role of multiple planktonic groups, *J. Geophys. Res.*, *112*, C08001, doi:10.1029/2006JC003852.

Fung, I. Y., S. K. Meyn, I. Tegen, S. C. Doney, J. G. John, and J. K. B. Bishop (2000), Iron supply and demand in the upper ocean, *Global Biogeochem. Cycles*, *14*(1), 281–295, doi:10.1029/1999GB900059.

Garcia, H. E., R. A. Locarnini, T. P. Boyer, and J. I. Antonov (2006a), *World Ocean Atlas 2005: Dissolved Oxygen, Apparent Oxygen Utilization, and Oxygen Saturation*, 342 pp., U.S. Government Printing Office, Washington, D. C.

Garcia, H. E., R. A. Locarnini, T. P. Boyer, and J. I. Antonov (2006b), *World Ocean Atlas 2005: Nutrients (phosphate, nitrate, silicate)*, U.S. Government Printing Office, Washington, D. C.

Gent, P. R., J. Willebrand, T. J. McDougall, and J. C. McWilliams (1995), Parameterizing eddy-induced tracer transports in ocean circulation models, *J. Phys. Oceanogr.*, *25*(4), 463–474, doi:10.1175/1520-0485(1995)025<0463:peitti>2.0.co;2.

Goebel, N. L., K. A. Turk, K. M. Achilles, R. Paerl, I. Hewson, A. E. Morrison, J. P. Montoya, C. A. Edwards, and J. P. Zehr (2010), Abundance and distribution of major groups of diazotrophic cyanobacteria and their potential contribution to N_2 fixation in the tropical Atlantic Ocean, *Environ. Microbiol.*, *12*(12), 3272–3289, doi:10.1111/j.1462-2920.2010.02303.x.

Goering, J. J., R. C. Dugdale, and D. W. Menzel (1966), Estimates of in situ rates of nitrogen uptake by *Trichodesmium* sp in the tropical Atlantic Ocean, *Limnol. Oceanogr.*, *11*(4), 614–620.

González Taboada, F., R. González Gil, J. Höfer, S. González, and R. Anadón (2010), *Trichodesmium* spp. population structure in the eastern North Atlantic subtropical gyre, *Deep Sea Res., Part I*, *57*(1), 65–77, doi:10.1016/j.dsr.2009.09.005.

Groβkopf, T., W. Mohr, T. Baustian, H. Schunck, D. Gill, M. M. M. Kuypers, G. Lavik, R. A. Schmitz, D. W. R. Wallace, and J. LaRoche (2012), Doubling of marine dinitrogen-fixation rates based on direct measurements, *Nature*, *488*(7411), 361–364.

Gruber, N., and J. L. Sarmiento (1997), Global patterns of marine nitrogen fixation and denitrification, *Global Biogeochem. Cycles*, *11*, 235–266.

Hansell, D. A., N. R. Bates, and D. B. Olson (2004), Excess nitrate and nitrogen fixation in the North Atlantic Ocean, *Mar. Chem.*, *84*, 243–265.

Holl, C. M., and J. P. Montoya (2005), Interactions between nitrate uptake and nitrogen fixation in continuous cultures of the marine diazotroph *Trichodesmium* (cyanobacteria), *J. Phycology*, *41*, 1178–1183.
Hood, R. R., V. J. Coles, and D. G. Capone (2004), Modeling the distribution of *Trichodesmium* and nitrogen fixation in the Atlantic Ocean, *J. Geophys. Res.*, *109*, C06006, doi:10.1029/2002JC001753.
Hynes, A. M., P. D. Chappell, S. T. Dyhrman, S. C. Doney, and E. A. Webb (2009), Cross-basin comparison of phosphorus stress and nitrogen fixation in *Trichodesmium*, *Limnol. Oceanogr.*, *54*(5), 1438–1448, doi:10.4319/lo.2009.54.5.1438.
Karl, D. M., M. J. Church, J. E. Dore, R. M. Letelier, and C. Mahaffey (2012), Predictable and efficient carbon sequestration in the North Pacific Ocean supported by symbiotic nitrogen fixation, *Proc. Natl. Acad. Sci. U. S. A.*, *109*(6), 1842–1849, doi:10.1073/pnas.1120312109.
Karl, D., R. Letelier, L. Tupas, J. Dore, J. Christian, and D. Hebel (1997), The role of nitrogen fixation in biogeochemical cycling in the subtropical North Pacific Ocean, *Nature*, *388*, 533–538.
Karl, D., A. Michaels, B. Bergman, D. G. Capone, E. J. Carpenter, R. Letelier, F. Lipshultz, H. W. Paerl, D. Stigman, and L. Stahl (2002), Dinitrogen fixation in the world's oceans, *Biogeochemistry*, *57*(58), 47–98.
Knapp, A. N., P. J. DiFiore, C. Deutsch, D. M. Sigman, and F. Lipschultz (2008), Nitrate isotopic composition between Bermuda and Puerto Rico: Implications for N_2 fixation in the Atlantic Ocean, *Global Biogeochem. Cycles*, *22*, GB3014, doi:10.1029/2007GB003107.
Krauk, J. M., T. A. Villareal, J. A. Sohm, J. P. Montoya, and D. G. Capone (2006), Plasticity of N:P ratios in laboratory and field populations of *Trichodesmium* spp, *Aquat. Microb. Ecol.*, *42*(3), 243–253, doi:10.3354/ame042243.
Landrum, J. P., M. A. Altabet, and J. P. Montoya (2011), Basin-scale distributions of stable nitrogen isotopes in the subtropical North Atlantic Ocean: Contribution of diazotroph nitrogen to particulate organic matter and mesozooplankton, *Deep Sea Res., Part I*, *58*(5), 615–625, doi:10.1016/j.dsr.2011.01.012.
Large, W. G., and S. G. Yeager (2004), Diurnal to decadal global forcing for ocean and sea-ice models: The data sets and flux climatologies, NCAR Technical Note NCAR/TN-460 + STR *Rep.*, 1–113 pp., NCAR, Boulder, Colo.
LaRoche, J., and E. Breitbarth (2005), Importance of the diazotrophs as a source of new nitrogen in the ocean, *J. Sea Res.*, *53*(1–2), 67–91, doi:10.1016/j.seares.2004.05.005.
Lenes, J. M., J. J. Walsh, D. B. Otis, and K. L. Carder (2005), Iron fertilization of *Trichodesmium* off the west coast of Barbados: A one-dimensional numerical model, *Deep Sea Res., Part I*, *52*, 1021–1041.
Letelier, R. M., and D. M. Karl (1998), *Trichodesmium* spp. physiology and nutrient fluxes in the North Pacific subtropical gyre, *Aquat. Microb. Ecol.*, *15*, 265–276.
Lipschultz, F., and N. J. P. Owens (1996), An assessment of nitrogen fixation as a source of nitrogen to the North Atlantic Ocean, *Biogeochemistry*, *35*, 261–274.
Luo, Y.-W., et al. (2012), Database of diazotrophs in global ocean: abundance, biomass and nitrogen fixation rates, *Earth Syst. Sci. Data*, *4*, 47–73, doi:10.5194/essd-4-47-2012.
Mahowald, N. M., A. R. Baker, G. Bergametti, N. Brooks, R. A. Duce, T. D. Jickells, N. Kubilay, J. M. Prospero, and I. Tegen (2005), Atmospheric global dust cycle and iron inputs to the ocean, *Global Biogeochem. Cycles*, *19*, GB4025, doi:10.1029/2004GB002402.
Mather, R. L., S. E. Reynolds, G. A. Wolff, R. G. Williams, S. Torres-Valdes, E. M. S. Woodward, A. Landolfi, X. Pan, R. Sanders, and E. P. Achterberg (2008), Phosphorus cycling in the North and South Atlantic Ocean subtropical gyres, *Nat. Geosci.*, *1*(7), 439–443.
McGillicuddy, D. J., L. A. Anderson, S. C. Doney, and M. E. Maltrud (2003), Eddy-driven sources and sinks of nutrients in the upper ocean: Results from a 0.1° resolution model of the North Atlantic, *Global Biogeochem. Cycles*, *17*(2), 1035, doi:10.1029/2002GB001987.
Michaels, A. F., D. Olson, J. L. Sarmiento, J. W. Ammerman, K. Fanning, R. Jahnke, A. H. Knap, F. Lipschultz, and J. M. Prospero (1996), Inputs, losses and transformations of nitrogen and phosphorus in the pelagic North Atlantic Ocean, *Biogeochemistry*, *35*, 181–226.
Mills, M. M., C. Ridame, M. Davey, J. La Roche, and R. J. Geider (2004), Iron and phosphorus co-limit nitrogen fixation in the eastern tropical North Atlantic, *Nature*, *429*(6989), 292–294.
Monteiro, F. M., M. J. Follows, and S. Dutkiewicz (2010), Distribution of diverse nitrogen fixers in the global ocean, *Global Biogeochem. Cycles*, *24*, GB3017, doi:10.1029/2009GB003731.
Monteiro, F. M., S. Dutkiewicz, and M. J. Follows (2011), Biogeographical controls on the marine nitrogen fixers, *Global Biogeochem. Cycles*, *25*, GB2003, doi:10.1029/2010GB003902.
Montoya, J. P., E. J. Carpenter, and D. G. Capone (2002), Nitrogen fixation and nitrogen isotope abundances in zooplankton of the oligotrophic North Atlantic, *Limnol. Oceanogr.*, *47*(6), 1617–1628, doi:10.4319/lo.2002.47.6.1617.
Moore, C. M., et al. (2009), Large-scale distribution of Atlantic nitrogen fixation controlled by iron availability, *Nat. Geosci.*, *2*(12), 867–871.
Moore, J. K., and O. Braucher (2008), Sedimentary and mineral dust sources of dissolved iron to the world ocean, *Biogeosciences*, *5*, 631–656, doi:10.5194/bg-5-631-2008.
Moore, J. K., and S. C. Doney (2007), Iron availability limits the ocean nitrogen inventory stabilizing feedbacks between marine denitrification and nitrogen fixation, *Global Biogeochem. Cycles*, *21*, GB2001, doi:10.1029/2006GB002762.
Moore, J. K., S. C. Doney, J. C. Kleypas, D. M. Glover, and I. Y. Fung (2002), An intermediate complexity marine ecosystem model for the global domain, *Deep Sea Res., Part II*, *49*, 403–462.
Moore, J. K., S. C. Doney, and K. Lindsay (2004), Upper ocean ecosystem dynamics and iron cycling in a global three-dimensional model, *Global Biogeochem. Cycles*, *18*, GB4028, doi:10.1029/2004GB002220.
Moore, J. K., S. C. Doney, K. Lindsay, N. Mahowald, and A. F. Michaels (2006), Nitrogen fixation amplifies the ocean biogeochemical response to decadal timescale variations in mineral dust deposition, *Tellus*, *58B*, 560–572.
Moore, J. K., K. Lindsay, S. C. Doney, M. C. Long, and K. Misumi (2013), Marine ecosystem dynamics and biogeochemical cycling in the Community Earth System Model [CESM1(BGC)]: Comparison of the 1990s with the 2090s under the RCP4.5 and RCP8.5 scenarios, *J. Clim.*, *26*, 9291–9312, doi:10.1175/jcli-d-12-00566.1.
Mulholland, M. R. (2007), The fate of nitrogen fixed by diazotrophs in the ocean, *Biogeosciences*, *4*, 37–51.
Mulholland, M. R., K. Ohki, and D. G. Capone (2001), Nutrient controls on nitrogen uptake and metabolism by natural populations and cultures of *Trichodesmium* (cyanobacteria), *J. Phycology*, *37*(6), 1001–1009, doi:10.1046/j.1529-8817.2001.00080.x.
O'Neil, J. M., and M. R. Roman (1994), Ingestion of the cyanobacterium *Trichodesmium* spp. by pelagic harpacticoid copepods *Macrosetella*, *Miracia* and *Oculosetella*, *Hydrobiologia*, *292-293*(1), 235–240, doi:10.1007/bf00229946.
Orcutt, K. M., F. Lipschultz, K. Gundersen, R. Arimoto, A. F. Michaels, A. H. Knap, and J. R. Gallon (2001), A seasonal study of the significance of N_2 fixation by *Trichodesmium* spp. at the Bermuda Atlantic Time-series Study (BATS) site, *Deep Sea Res., Part II*, *48*, 1583–1608.
Oschlies, A., and V. C. Garcon (1999), An eddy-permitting coupled physical-biological model of the North Atlantic 1. Sensitivity to advection numerics and mixed layer physics, *Global Biogeochem. Cycles*, *13*, 135–160.
Palter, J. B., M. S. Lozier, J. L. Sarmiento, and R. G. Williams (2011), The supply of excess phosphate across the Gulf Stream and the maintenance of subtropical nitrogen fixation, *Global Biogeochem. Cycles*, *25*, GB4007, doi:10.1029/2010GB003955.

Richier, S., A. I. Macey, N. J. Pratt, D. J. Honey, C. M. Moore, and T. S. Bibby (2012), Abundances of iron-binding photosynthetic and nitrogen-fixing proteins of *Trichodesmium* both in culture and in situ from the North Atlantic, *PLoS ONE*, *7*(5), e35571, doi:10.1371/journal.pone.0035571.

Sañudo-Wilhelmy, S. A., A. Kustka, C. J. Gobler, M. Yang, D. A. Hutchins, J. Burns, D. Capone, J. H. Raven, and E. J. Carpenter (2001), Phosphorus limitation of nitrogen fixation by *Trichodesmium* in the Central Atlantic Ocean, *Nature*, *411*, 66–69.

Smith, R. D., M. E. Maltrud, F. O. Bryan, and M. W. Hecht (2000), Numerical simulation of the North Atlantic Ocean at 1/10 degree, *J. Phys. Oceanogr.*, *30*, 1532–1561.

Sohm, J. A., C. Mahaffey, and D. Capone (2008), Assessment of relative phosphorus limitation of *Trichodesmium* spp. in the North Pacific, North Atlantic, and north coast of Australia, *Limnol. Oceanogr.*, *53*(6), 2495–2502.

Subramaniam, A., et al. (2008), Amazon River enhances diazotrophy and carbon sequestration in the tropical North Atlantic Ocean, *Proc. Natl. Acad. Sci. U. S. A.*, *105*(30), 10,460–10,465, doi:10.1073/pnas.0710279105.

Tyrrell, T., E. Marañón, A. J. Poulton, A. R. Bowie, D. S. Harbour, and E. M. S. Woodward (2003), Large-scale latitudinal distribution of *Trichodesmium* spp. in the Atlantic Ocean, *J. Plankton Res.*, *25*(4), 405–416, doi:10.1093/plankt/25.4.405.

Van Mooy, B. A. S., L. R. Hmelo, L. E. Sofen, S. R. Campagna, A. L. May, S. T. Dyhrman, A. Heithoff, E. A. Webb, L. Momper, and T. J. Mincer (2012), Quorum sensing control of phosphorus acquisition in *Trichodesmium* consortia, *ISME J.*, *6*(2), 422–429, doi:10.1038/ismej.2011.115.

Ward, B. A., S. Dutkiewicz, C. M. Moore, and M. J. Follows (2013), Iron, phosphorus, and nitrogen supply ratios define the biogeography of nitrogen fixation, *Limnol. Oceanogr.*, *58*(6), 2059–2075, doi:10.4319/lo.2013.58.6.2059.

Webb, E. A., J. W. Moffett, R. Wisniewski, and S. T. Dyhrman (2007), Molecular assessment of phosphorus and iron physiology in *Trichodesmium* populations from the western central and western south Atlantic, *Limnol. Oceanogr.*, *52*, 2221–2232.

Westberry, T. K., and D. A. Siegel (2006), Spatial and temporal distribution of *Trichodesmium* blooms in the world's oceans, *Global Biogeochem. Cycles*, *20*, GB4016, doi:10.1029/2005GB002673.

White, A. E., Y. H. Spitz, D. M. Karl, and R. M. Letelier (2006), Flexible elemental stoichiometry in *Trichodesmium* spp. and its ecological implications, *Limnol. Oceanogr.*, *51*(4), 1777–1790.

Zehr, J. P. (2011), Nitrogen fixation by marine cyanobacteria, *Trends Microbiol.*, *19*(4), 162–173, doi:10.1016/j.tim.2010.12.004.

Auxiliary Material for

Do *Trichodesmium* spp. populations in the North Atlantic export most of the nitrogen they fix?

Dennis J. McGillicuddy, Jr.
Department of Applied Ocean Physics and Engineering
Woods Hole Oceanographic Institution
Woods Hole, MA 02543, USA

Corresponding author: D.J. McGillicuddy, Jr. (dmcgillicuddy@whoi.edu)

Global Biogeochemical Cycles, 2013

This document provides supplementary information describing the model used in the main article, as well as comparisons with a prior solution described in Anderson et al. [2011].

Contents:

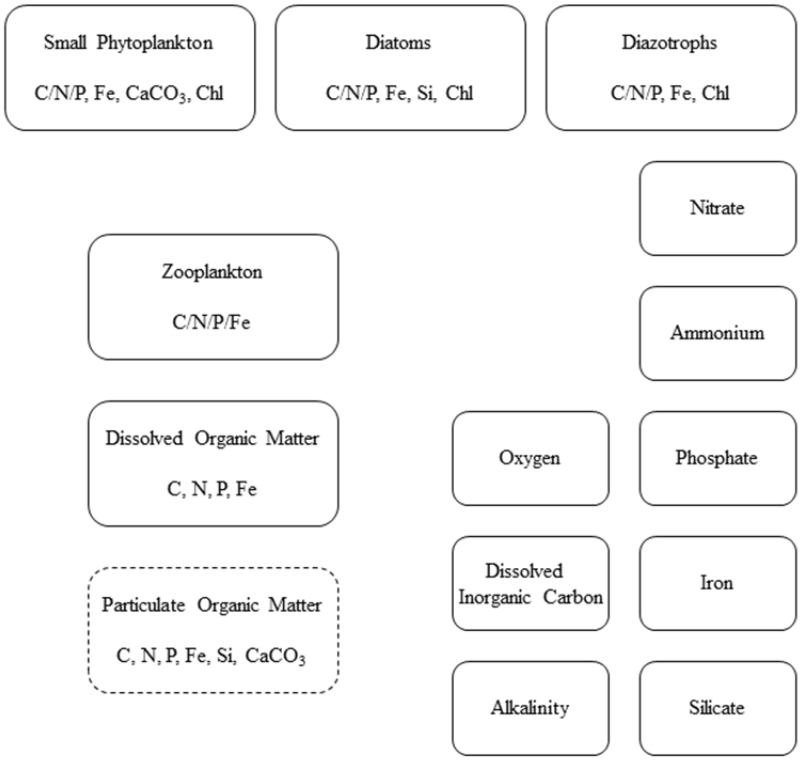

Figure S1. The BEC model as described by Moore and Doney [2007] and Moore et al. [2006]. The dashed box for particulate organic matter reflects the fact that it is not a true state variable, insofar as that material is assumed to sink and remineralize instantly.

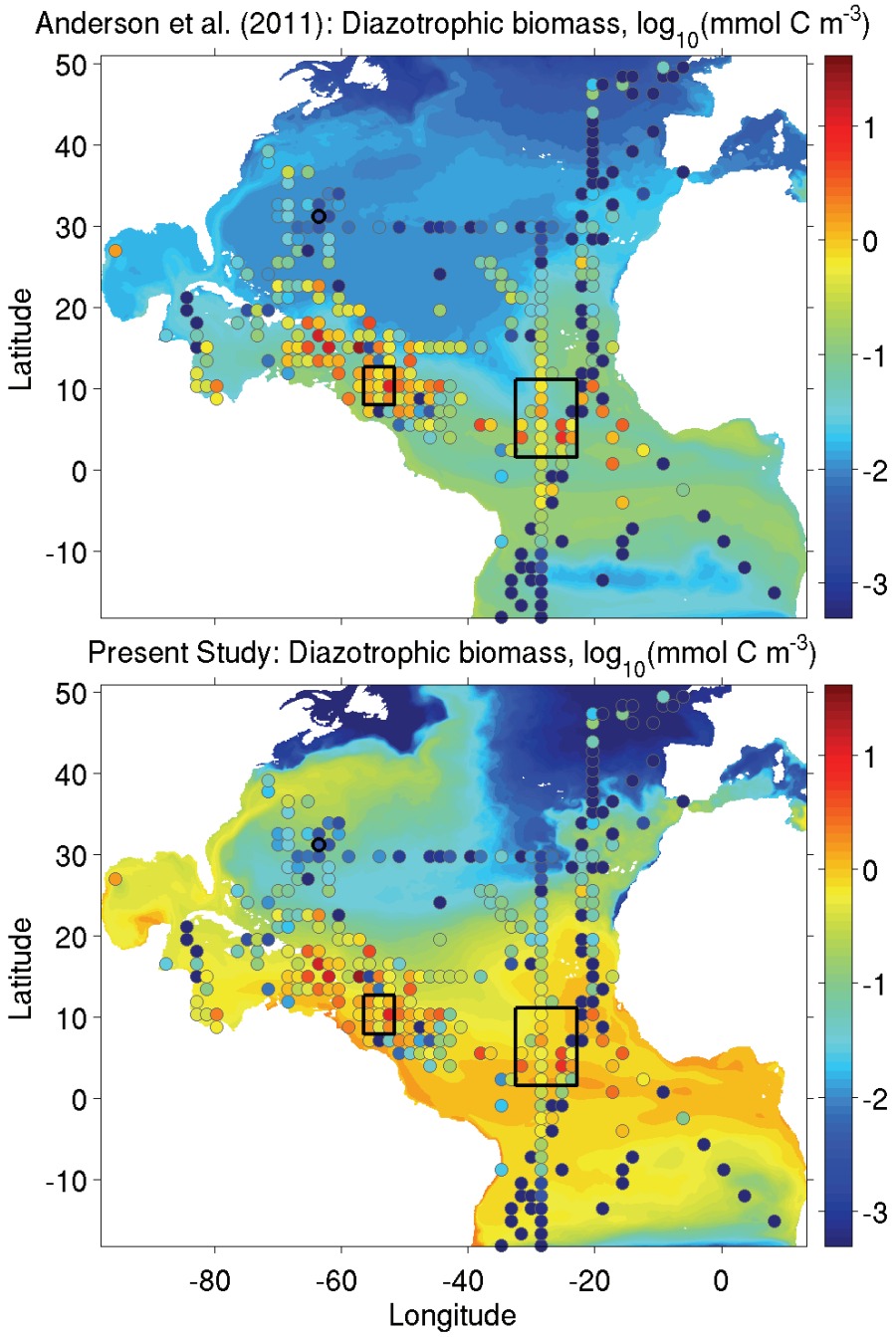

Figure S2. Near-surface (0-10 m) diazotrophic biomass for the Anderson et al. [2011] solution (top) and new biological model (bottom). Data from Luo et al. [2012], binned onto the 1.6° model grid, are shown as colored circles. Outlined in black are the locations of BATS (circle near 32°N 64°W), as well as Tropical West (rectangle centered at 10°N 54°W) and Tropical East (rectangle centered at 6°N 28°W) domains, for which detailed flux diagnosis is presented in Figure 6.

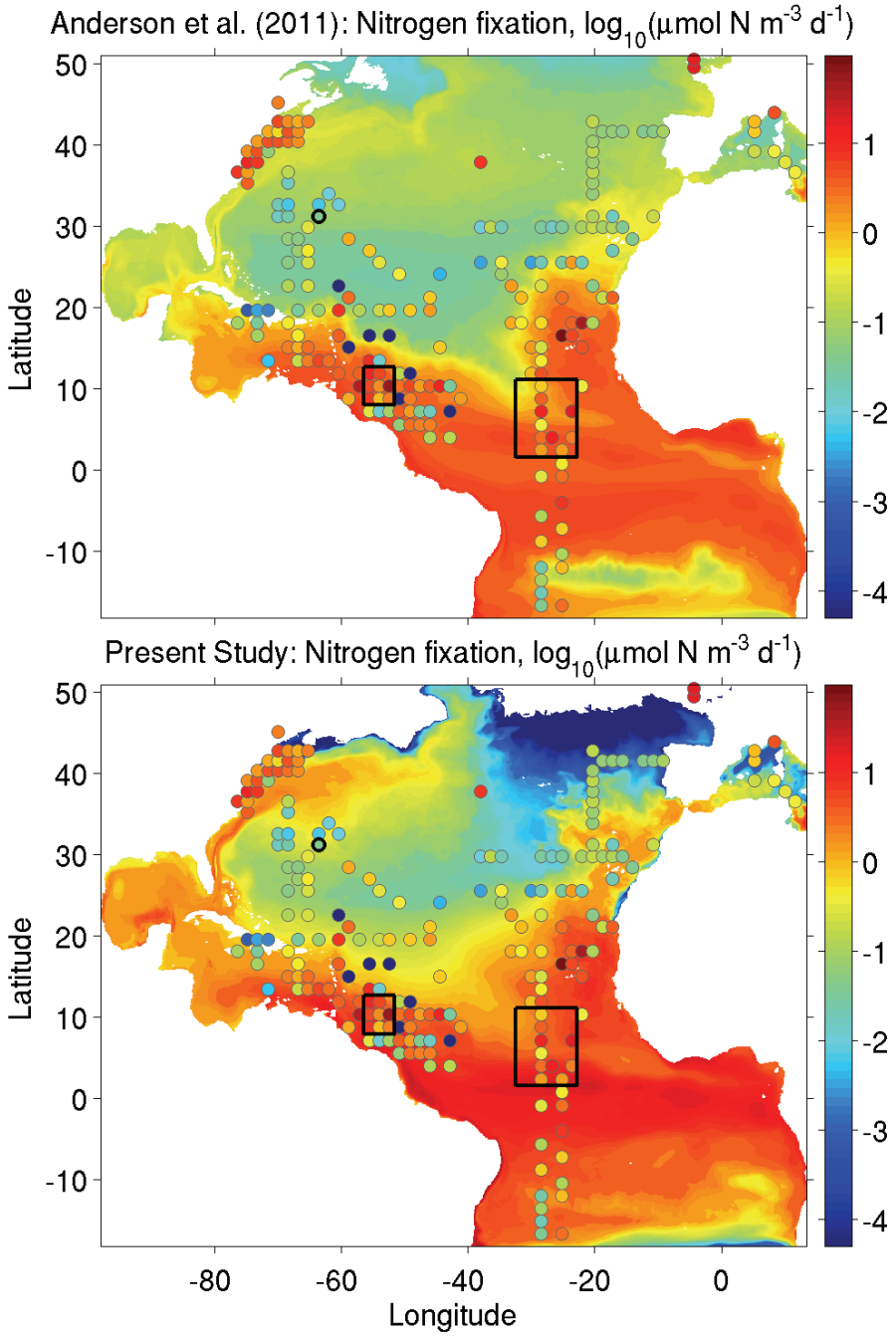

Figure S3. Near-surface (0-10 m) nitrogen fixation for the Anderson et al. [2011] solution (top) and new biological model (bottom). Data from Luo et al. [2012], binned onto the 1.6° model grid, are shown as colored circles. Outlined in black are the locations of BATS (circle near 32°N 64°W), as well as Tropical West (rectangle centered at 10°N 54°W) and Tropical East (rectangle centered at 6°N 28°W) domains, for which detailed flux diagnosis is presented in Figure 6.

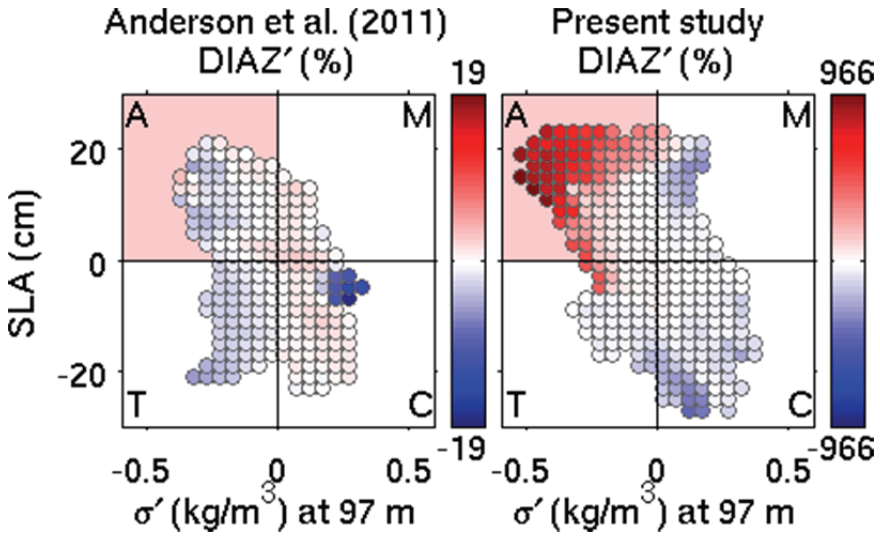

Figure S4. Vertically integrated (0–104 m) diazotrophic biomass anomalies (mg C m^{-2}), expressed as percent anomaly from the large-scale mean, binned according to SLA and *in situ* density anomaly at 97 m in the subdomain bordered by the white rectangle in Figure 8 (30-35°N, 30-48°W). The four quadrants correspond to anticyclones (A), mode-water eddies (M), thinnies (T) and cyclones (C). The background shading indicates the observed correlations in this region, which suggest enhancement of *Trichodesmium* spp. populations in anticyclones [*Davis and McGillicuddy*, 2006]. Left: the solution from Anderson et al. [2011]; right: the new model. For consistency with the observations, analysis of the model output is restricted to the August-September time frame.

Table S1: Selected parameters of the ecosystem model. Changes from the Anderson et al. [2011] model are highlighted in bold.

Parameter	Definition	Anderson et al. [2011] (Run 14)	This model (Run 63)
sp_kNO3	Half saturation constant for nitrate uptake by diazotrophs	0.5	0.5 μM N
diat_kNO3	″ nitrate uptake by diatoms	2.5	2.5 μM N
diaz_kNO3	″ nitrate uptake by diazotrophs	N/A	**1.0 μM N**
sp_kNH4	″ ammonium uptake by small phytoplankton	0.005	0.005 μM N
diat_kNH4	″ ammonium uptake by diatoms	0.08	0.08 μM N
diaz_kNH4	″ ammonium uptake by diazotrophs	N/A	**0.1 μM N**
sp_kPO4	″ phosphate uptake by small phytoplankton	0.005 μM P	0.005 μM P
diat_kPO4	″ phosphate uptake by diatoms	0.02 μM P	0.02 μM P
diaz_kPO4	″ phosphate uptake by diazotrophs	0.005 μM P	0.005 μM P
diat_kFe	″ iron uptake by diatoms	0.15 nM Fe	**0.08 nM Fe**
diaz_kFe	″ iron uptake by diazotrophs	0.1 nM Fe	**0.8 nM Fe**
fe_max_scale2	Iron scavenging coefficient	4286 (μM Fe yr)$^{-1}$	**20000 (μM Fe yr)$^{-1}$**
loss_thres_diaz	Threshold for diazotrophic loss terms	0.01 μM C	**0.001 μM C**
diaz_umax_0	Maximum growth rate of diazotrophs	1.2 d^{-1}	**0.1 d^{-1}**
diaz_mort	Coefficient of linear diazotrophic mortality	0.16 d^{-1}	**0.02 d^{-1}**
diaz_mort2	Coefficient of quadratic diazotrophic mortality	0	**0.0324 (μM C d)$^{-1}$**
r_Nfix_photo	Ratio of nitrogen fixation to assimilation	1.43	**1.0***
f_diaz_loss_poc	Fraction of linear diazotrophic mortality going to POCt	0	**1.0**
f_graze_diaz_poc	Fraction of diazotrophic grazing loss going to POCt	0	**0.275**
POCt_diss	Length scale for diazotroph POC remineralization	N/A	**300 m**

*The decrease in r_Nfix_photo from 1.43 to 1.0 was an attempt to alleviate the unrealistic buildup of nitrate by eliminating the excess amount of fixed N_2 excreted as DON, which is in turn remineralized to nitrate. This proved to have little impact on the solutions. Future versions of the model should include DON excretion by diazotrophs, as there is ample evidence that *Trichodesmium* spp. do just that [*Glibert and Bronk*, 1994; *Mulholland et al.*, 2004].

References

Anderson, L. A., D. J. McGillicuddy, M. E. Maltrud, I. D. Lima, and S. C. Doney (2011), Impact of eddy–wind interaction on eddy demographics and phytoplankton community structure in a model of the North Atlantic Ocean, *Dynamics of Atmospheres and Oceans*, *52*(1-2), 80-94, doi:10.1016/j.dynatmoce.2011.01.003.

Davis, C. S., and D. J. McGillicuddy (2006), Transatlantic Abundance of the N_2-Fixing Colonial Cyanobacterium *Trichodesmium*, *Science*, *312*, 1517-1520.

Glibert, P. M., and D. A. Bronk (1994), Release of dissolved organic nitrogen by marine diazotrophic cyanobacteria, *Trichodesmium* spp., *Applied Environmental Microbiology*, *60*, 3996-4000.

Luo, Y.-W., S. C. Doney, L. A. Anderson, M. Benavides, I. Berman-Frank, A. Bode, S. Bonnet, K. H. Boström, D. Böttjer, D. G. Capone, E. J. Carpenter, Y. L. Chen, M. J. Church, J. E. Dore, L. I. Falcón, A. Fernández, R. A. Foster, K. Furuya, F. Gómez, K. Gundersen, A. M. Hynes, D. M. Karl, S. Kitajima, R. J. Langlois, J. LaRoche, R. M. Letelier, E. Marañón, D. J. McGillicuddy, P. H. Moisander, C. M. Moore, B. Mouriño-Carballido, M. R. Mulholland, J. A. Needoba, K. M. Orcutt, A. J. Poulton, E. Rahav, P. Raimbault, A. P. Rees, L. Riemann, T. Shiozaki, A. Subramaniam, T. Tyrrell, K. A. Turk-Kubo, M. Varela, T. A. Villareal, E. A. Webb, A. E. White, J. Wu, and J. P. Zehr (2012), Database of diazotrophs in global ocean: abundance, biomass and nitrogen fixation rates, *Earth System Science Data*, *4*, 47–73, doi:doi:10.5194/essd-4-47-2012.

Moore, J. K., and S. C. Doney (2007), Iron availability limits the ocean nitrogen inventory stabilizing feedbacks between marine denitrification and nitrogen fixation, *Global Biogeochemical Cycles*, *21*(GB2001), doi:10.1029/2006GB002762,2007.

Moore, J. K., S. C. Doney, K. Lindsay, N. Mahowald, and A. F. Michaels (2006), Nitrogen fixation amplifies the ocean biogeochemical response to decadal timescale variations in mineral dust deposition, *Tellus*, *58B*, 560-572.

Mulholland, M. R., D. A. Bronk, and D. G. Capone (2004), Dinitrogen fixation and release of ammonium and dissolved organic nitrogen by Trichodesmium IMS101, *Aquatic Microbial Ecology*, *37*(1), 85-94, doi:10.3354/ame037085.